Journal of Alloys and Compounds 509 (2011) 2885–2890

Contents lists available at ScienceDirect

Journal of Alloys and Compounds

journal homepage: www.elsevier.com/locate/jallcom

Structural, elastic and electronic properties of $Mg(Cu_{1-x}Zn_x)_2$ alloys calculated by first-principles

Meng-Meng Wu[a], Yi Jiang[a], Ji-Wei Wang[b], Jian Wu[b], Bi-Yu Tang[a,b,*], Li-Ming Peng[c], Wen-Jiang Ding[c]

[a] School of Chemistry and Chemical Engineering, Guangxi University, Nanning 530004, China
[b] Department of Physics, Xiangtan University, Hunan Province 411105, China
[c] Light Alloy Net Forming National Engineering Research Center, School of Materials Science and Engineering, Shanghai Jiaotong University, Shanghai 200030, China

ARTICLE INFO

Article history:
Received 10 August 2010
Received in revised form
19 November 2010
Accepted 22 November 2010
Available online 1 December 2010

Keywords:
$Mg(Cu_{1-x}Zn_x)_2$ alloys
Elastic properties
Mechanical properties
Electronic structure
First-principle calculations

ABSTRACT

The structural, elastic and electronic properties of $Mg(Cu_{1-x}Zn_x)_2$ alloys ($x = 0$, 0.25, 0.5,and 0.75) were investigated by means of first-principle calculations within the framework of density functional theory (DFT). The calculation results demonstrated that the partial substitution of Cu with Zn in $MgCu_2$ leaded to an increase of lattice constants, and the optimized structural parameters were in very good agreement with the available experimental values. From energetic point of view, it was found that with increase of Zn content the structural stability of $Mg(Cu_{1-x}Zn_x)_2$ alloys decreased apparently. The single-crystal elastic constants were obtained by computing total energy as a function of strain, and then the bulk modulus B, shear modulus G, Young's modulus Y and Poisson's ratio ν of polycrystalline aggregates were derived. The calculated results showed that among the $Mg(Cu_{1-x}Zn_x)_2$ alloys, MgCuZn exhibited the largest stiffness, while Mg_2Cu_3Zn showed the best ductility. Finally, the electronic density of states (DOSs) and charge density distribution were further studied and discussed.

1. Introduction

Mg-based alloys have low density, good stiffness and the high strength-to-weight ratio [1,2]. The weight of typical magnesium alloys is 35% lower than that of their aluminum counterparts at equal stiffness [3], so Mg-based alloys have been more and more attractive in industrial applications due to their lightweight properties and abundance of resources [4,5]. However, their applications are also restricted because of the limited tensile strength and inferior ductility. Hence, there is an urgent need to improve the mechanical property of magnesium alloys, and much effort has been devoted to developing high-strength magnesium alloys with good ductility [6,7].

The addition of rare-earth (RE) elements has been known to improve the mechanical properties of magnesium alloys owing to the formation of strengthening precipitates [8–10], which play a very important role in optimizing the microstructure [11–13]. However, the cost of RE elements is high. Recent investigations have shown that the addition of Cu can overcome the drawback of brittleness for Mg-based alloys [14,15], and it is also found that the Mg–Cu alloys exhibit age-hardening response [16]. On the other hand, the addition of Zn can improve the plasticity of high-strength and electrical properties of Mg–Cu alloys effectively [14,15]. Particularly, addition of Cu and Zn elements to Mg alloys can improve the solid-solution strengthening and the age-hardening at both room and elevated temperature, so further theoretical and experimental study is necessary.

The elastic constants determine the response of the crystal to external forces, as characterized by the bulk modulus, shear modulus, Young's modulus and Poisson's ratio, so play an important role in determining the mechanical properties of solid materials [17]. Over the past decade, much effort has been made to calculate the elastic constants from first-principles calculations, especially for the cubic materials [18,19]. These investigations will provide valuable guidance for analysis and design of alloys [18–23]. However, to the best of our knowledge, theoretical investigation on the elastic and electronic properties of $Mg(Cu_{1-x}Zn_x)_2$ alloys has not yet been reported.

In this paper, we performed a systematic investigation of the structural, elastic and electronic properties on face-centered cubic (fcc) precipitates of $Mg(Cu_{1-x}Zn_x)_2$ alloys by first-principle calculations, and the calculated results were discussed in comparison with the available experimental data.

2. Computational method

The present calculations were performed using density functional theory (DFT) [24] as implemented in the Vienna Ab Initio Simulation Package (VASP) code [25]. The Perdew–Wang (PW91)

* Corresponding author at: School of Chemistry and Chemical Engineering, Guangxi University, Nanning 530004, China.
E-mail addresses: tangbiyu@gxu.edu.cn, tangbiyu@xtu.edu.cn (B.-Y. Tang).

0925-8388/$ – see front matter © 2010 Elsevier B.V. All rights reserved.
doi:10.1016/j.jallcom.2010.11.148

version of the generalized gradient approximation (GGA) [26] was used to describe the exchange-correlation energy functional and the projector augmented wave (PAW) method [27] had been used in the present work. The electron configuration for Mg treated 3 s states as valence state, and others were described by 3d, 4s valence states for Zn and Cu, respectively. The cutoff energy of plane wave was set at 350 eV for $Mg(Cu_{1-x}Zn_x)_2$ alloys. The Brillouin zone integrations used Monkhorst-Pack grids [28] of $9 \times 9 \times 9$ mesh for optimizing geometry and calculating elastic constants, and $12 \times 12 \times 12$ for calculation of the density of states (DOSs). The geometry optimization was performed by full relaxation until the total energy changes within 10^{-4} eV/atom and the Hellmann–Feynman force on all atoms was less than 10^{-2} eV/Å. The density of states (DOSs) and total energy calculations were performed using the linear tetrahedron method with Blöchl correction [29].

3. Results and discussion

3.1. Structures and lattice constants

$MgCu_2$ has a cubic structure with the space group of $Fd\bar{3}m$, which is denoted by a Pearson symbol of *cF24*. The unit cell of $MgCu_2$ contains 8 Mg atoms and 16 Cu atoms, and the lattice constant is 0.704 nm [30]. By Zn doping, the ternary cubic Laves phases $Mg(Cu,Zn)_2$ are obtained [31]. In order to investigate the structure and elastic properties of the ternary cubic Laves phase $Mg(Cu,Zn)_2$, Cu atoms were partially replaced by Zn atoms according to the symmetric position of space group to form Mg_2Cu_3Zn, MgCuZn and Mg_2CuZn_3, and the corresponding percentage of Zn doping in $MgCu_2$ were about 17 at.%, 33 at.%, 50 at.%, respectively. The Mg_2Cu_3Zn, MgCuZn and Mg_2CuZn_3 resulting from partial substitution of Cu with Zn in $MgCu_2$ still keep its fcc structure [31]. Starting from the above fcc structure model, the lattice parameters were first optimized with the full relaxation of cell volume and shape as well as atomic positions. The equilibrium parameters and bulk modulus B_0 of these alloys were determined by fitting the total energy calculated at different lattice constant to a Birch–Murnaghan equation of state (EOS) [32]. Then the lattice constant a and volume V_0 for $Mg(Cu_{1-x}Zn_x)_2$ alloys were derived and listed in Table 1, where the available experimental and theoretical results were also presented. It can be seen that the calculated lattice constant of $MgCu_2$ phase agreed very well with the experimental and theoretical data [30,33]. Although there were no available experimental measurements of lattice constants for Mg_2Cu_3Zn, MgCuZn, Mg_2CuZn_3, it was very clear that the lattice constant a increased with Zn content increasing. The volume variations in Table 1 suggested that the Zn–Zn and Zn–Cu bonds were longer than Cu–Cu, which was consistent with analysis of electronic structures. The obtained bulk modulus B_0 as a function of Zn content is shown in Fig. 1. The results demonstrated that with increase of Zn content, the bulk modulus B_0 of these alloys dropped rapidly, and $MgCu_2$ had the maximum B_0 value. Since bulk modulus determined incompressibility, so the incompressibility of $Mg(Cu_{1-x}Zn_x)_2$ alloys reduced with Zn content increasing.

Table 1
The lattice parameter and the volume for $Mg(Cu_{1-x}Zn_x)_2$.

Compound	Lattice parameters (Å)		V_0 (Å^3)
	Experiment [Ref.]	Ab initio (this study) [Ref.]	
$MgCu_2$	a = 7.04 [30]	a = 7.04674 and 7.03525 [33]	349.94
Mg_2Cu_3Zn	–	a = 7.1114	359.64
MgCuZn	–	a = 7.1726	369.92
Mg_2CuZn_3	–	a = 7.264	383.29

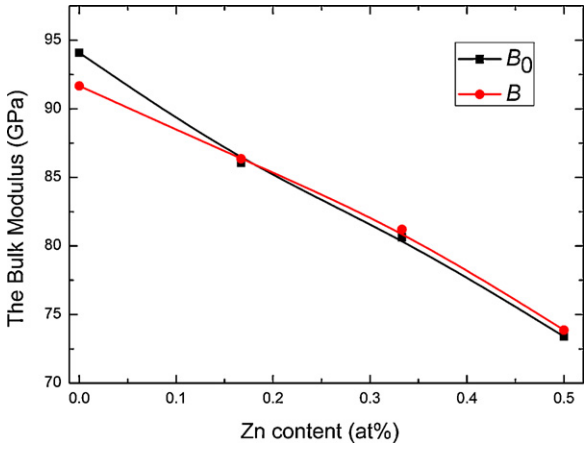

Fig. 1. The bulk modulus B derived from the values of the elastic constants and the B_0 obtained through the Birch–Murnaghan EOS.

It is known that the cohesive energy is a measure of the force to bind atoms together in the solid state, so it shows the structural stability of the alloys. The cohesive energy E_{coh} per atom for $Mg(Cu_{1-x}Zn_x)_2$ alloys can be calculated by

$$E_{coh} = \frac{E_{tot} - N_A E^A_{atom} - N_B E^B_{atom} - N_C E^C_{atom}}{N_A + N_B + N_C} \quad (1)$$

where E_{tot} is the total energy of the unit cell used in the present calculation, E^A_{atom}, E^B_{atom} and E^C_{atom} are the energy of the isolated atoms A, B and C in the free state, respectively. N_A, N_B and N_C refer to the number of A, B and C atoms in unit cell, respectively. Fig. 2 shows the calculated cohesive energy E_{coh} of $Mg(Cu_{1-x}Zn_x)_2$ alloys. It can be found that the calculated E_{coh} for all these alloys increased with Zn content increasing. That was, the structural stability of $Mg(Cu_{1-x}Zn_x)_2$ alloys reduced with the Zn content increasing. Therefore, $MgCu_2$ was the most stable in $Mg(Cu_{1-x}Zn_x)_2$ alloys, whereas Mg_2CuZn_3 was the least stable. It was also found that there was a close relationship between E_{coh} and V_0, the more negative the E_{coh}, the stronger the atomic bonds, and the shorter the distance of neighboring atoms. As a result, the $Mg(Cu_{1-x}Zn_x)_2$ alloys with a low Zn content had a small V_0 but a high stability.

3.2. Elastic properties

Elastic constants are the measure of the resistance of a crystal to an externally applied stress. Generally, the single-crystal elastic constants can be obtained by calculating the total energy as a function of appropriate lattice deformation. Depending on the crystal

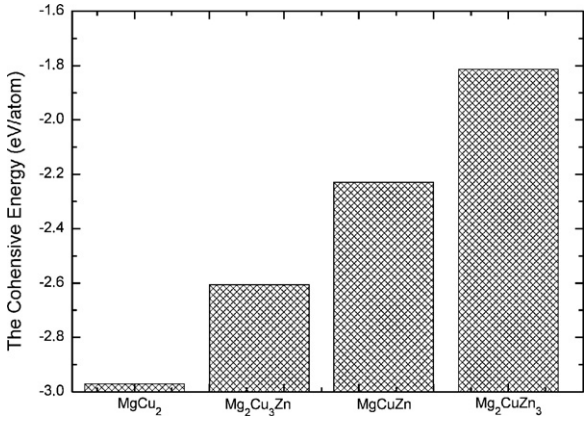

Fig. 2. The cohesive energy E_{coh} of $Mg(Cu_{1-x}Zn_x)_2$ alloys.

Table 2
The strains used to calculate the elastic constants of $Mg(Cu_{1-x}Zn_x)_2$ with $\delta = \pm 0.01n$ (n = 0–2). ΔE is the difference in energy between the strained lattice and the unstrained lattice.

Strain	Parameters (unlisted $e_i = 0$)	$\Delta E/V_0$
1	$e_1 = e_2 = \delta$, $e_3 = (1+\delta)^{-2} - 1$	$3\delta^2(C_{11} - C_{12})$
2	$e_1 = e_2 = e_3 = \delta$	$3\delta^2(C_{11} + 2C_{12})/2$
3	$e_6 = \delta$, $e_3 = \delta^2(4 - \delta^2)^{-1}$	$\delta^2 C_{44}/2$

symmetry and the type of lattice deformation imposed, the curvature of the total energy versus strain curves can define either a particular elastic constant or a combination of elastic constants. The internal energy ($E(V, \{e_i\})$) of a crystal under an infinitesimal strain e_i, with respect to the energy $E(V_0, 0)$ of the unstrained geometry, can be written as

$$E(V, \{e_i\}) = E(V_0, 0) + \frac{V_0}{2}\sum_{ij} C_{ij}e_i e_j + \cdots, \quad (2)$$

where V_0 is the volume of the unstrained system with $E(V_0, 0)$ being the corresponding energy, C_{ij}s are the single-crystal elastic constants and the strain tensor $\varepsilon = \{e_i, e_j, \ldots\}$ is given in Voigt notation. For a material with cubic symmetry, there are only three independent elastic constants, C_{11}, C_{12} and C_{44}. In order to obtain the elastic constants of the cubic crystal, three kinds of strains $\varepsilon^{(M)}$ (M = 1, 2,and 3) were applied, as listed in Table 2. The first one is a volume-conserving stretch along the z-axis, the second is equivalent to simple hydrostatic pressure, and the last strain corresponds to a volume-conserving monoclinic shear about the z-axis [18]. The calculated C_{ij}s of fcc $Mg(Cu_{1-x}Zn_x)_2$ alloys are listed in Table 3. It can be seen that for Mg_2Cu_3Zn and MgCuZn, the calculated elastic constants C_{11}, C_{12} and C_{44} were 120.02, 69.53, 38.01 and 142.53, 50.55, 64.97 GPa, respectively, while the experiment values of $Mg(Cu,Zn)_2$ for corresponding percentage of Zn doping are 118.60, 70, 41.90 and 144.15, 49.95, 62.85 GPa, respectively, indicating the calculated results agreed well with the experimental values. The obtained constants meet the requirements of mechanical stability for a cubic crystal [34]: $(C_{11} - C_{12}) > 0$, $C_{11} > 0$, $C_{44} > 0$,and $C_{12} > 0$. Therefore, these alloys were all mechanically stable phases. The present results also revealed the variation feature of C_{ij}s with different Zn content. It can be seen that C_{12} of $Mg(Cu_{1-x}Zn_x)_2$ dropped rapidly with addition of Zn, and C_{12} of $MgCu_2$ exhibited the maximum value. For C_{11} and C_{44}, MgCuZn possessed the maximum values while Mg_2Cu_3Zn had the minimum. The variation feature of C_{ij}s for $Mg(Cu_{1-x}Zn_x)_2$ alloys with Zn content in the present calculation were in accordance with the experimental values [31].

For polycrystalline samples, an averaged bulk modulus B and shear modulus G can be determined by combining values of the single-crystal C_{ij} according to the proper symmetry relations. Here Hershey's averaging method [35] was adopted, because it has been turned out to give the most accurate relation between single-crystal and polycrystalline data [36]. Then, the average shear modulus G is given by the solution of the cubic equation

$$G^3 + \alpha G^2 + \beta G + \gamma = 0 \quad (3)$$

$$\alpha = \frac{5C_{11} + 4C_{12}}{8} \quad (4)$$

Table 3
Calculated elastic constants (GPa) as well as polycrystalline the elastic parameters (G, Y, ν and A) for $Mg(Cu_{1-x}Zn_x)_2$.

Compound	C_{11}	C_{12}	C_{44}	B	G	G/B	Y	ν	A
$MgCu_2$	126.20	74.40	41.72	91.67	34.55	0.38	92.09	0.333	1.25
Mg_2Cu_3Zn	120.02	69.53	38.01	86.36	32.32	0.37	86.21	0.334	1.21
MgCuZn	142.53	50.55	64.97	81.21	56.60	0.87	137.78	0.217	1.27
Mg_2CuZn_3	121.54	50.04	56.39	73.87	47.03	0.64	116.39	0.237	1.34

$$\beta = -\frac{C_{44}(7C_{11} - 4C_{12})}{8} \quad (5)$$

$$\gamma = -\frac{C_{44}(C_{11} - C_{12})(C_{11} + 2C_{12})}{8} \quad (6)$$

The calculated results are listed in Table 3. It is well known that shear modulus is a measure of resistance to reversible deformations upon shear stress [37]. The larger is the value of shear modulus, the more pronounced is the directional bonding between atoms. The present calculated results demonstrated that MgCuZn had the largest shear modulus, and then followed by Mg_2CuZn_3, $MgCu_2$ and Mg_2Cu_3Zn. Hence, the directional bonding in MgCuZn would be the strongest for its largest shear modulus, and the directional bonding for Mg_2CuZn_3, $MgCu_2$ and Mg_2Cu_3Zn became weak due to the smaller shear modulus. For a cubic lattice the average bulk modulus is identical to the single-crystal bulk modulus, i.e., $B = (C_{11} + 2C_{12})/3$. Fig. 1 shows visually that the bulk modulus B of $Mg(Cu_{1-x}Zn_x)_2$ alloys decreased with Zn content increasing. It was also worth noting that, the bulk modulus B derived from the elastic constants agreed well with the B_0 obtained through the Birch–Murnaghan EOS, which gave a consistent estimation of the compressibility for these alloys. Young's modulus Y is defined as the ratio between stress and strain, and it can be given as $Y = 3BG/(3B + G)$ and used to provide a measure of the stiffness of the solid. The larger the value of Y is, the stiffer the material is. The calculated results in Table 3 indicated that the stiffness of MgCuZn was the largest, and then followed by Mg_2CuZn_3, $MgCu_2$ and Mg_2Cu_3Zn. The Poisson's ratio is also calculated as $\nu = (Y - 2G)/2G$, which can quantify the stability of the crystal against shear. The calculated results indicated that MgCuZn showed the lowest tenacity due to the smallest value of Poisson's ratio, Mg_2CuZn_3 had lower tenacity than $MgCu_2$ and Mg_2Cu_3Zn phases.

The ratio of the shear modulus to bulk modulus of crystalline phases introduced by Pugh [37] can predict the brittle and ductile behavior of materials. A high (low) G/B value was associated with brittleness (ductility). The critical value separating ductility from brittleness is about 0.57. The calculated results of Table 3 showed that MgCuZn exhibited a stronger brittleness than Mg_2CuZn_3, while Mg_2Cu_3Zn had better ductility than $MgCu_2$. The Pugh criterion of G/B is of high interest as it leads the path to engineering alloy design and is applied widely [38]. The random-texture elastic property homogenization could also be determined by G/B with complementation of upper and lower bound calculation [39].

The elastic anisotropy of crystals has an important implication in engineering science since it is highly correlated with the possibility of inducing microcracks in materials [40]. Therefore, the elastic anisotropy of these fcc $Mg(Cu_{1-x}Zn_x)_2$ alloys are predicted through anisotropy constant defined as $A = (2C_{44} + C_{12})/C_{11}$ for cubic symmetric structure [41]. If the material is completely isotropic, the value of A would be 1, while values smaller or bigger than 1 show the degree of elastic anisotropy [34]. It was interesting to note that the calculated values of A in Table 3 did not deviate far from unity, suggesting that these fcc $Mg(Cu_{1-x}Zn_x)_2$ alloys also did not deviate far from isotropy.

3.3. Electronic structure

Further analysis on the total and partial density of states (DOSs) of $Mg(Cu_{1-x}Zn_x)_2$ were performed to study how the electronic structure determined the structural stability and elastic properties. The calculated total and partial DOS are shown in Fig. 3, where the Fermi level was set at zero energy and marked by the vertical lines. As shown in Fig. 3, the DOS feature of the $Mg(Cu_{1-x}Zn_x)_2$ alloys was largely similar, the Cu-d states, Zn-p and Zn-d states, Mg-s and Mg-p states were broadly distributed in the entire region, while Cu-s states and Cu-p states were very weak in whole region.

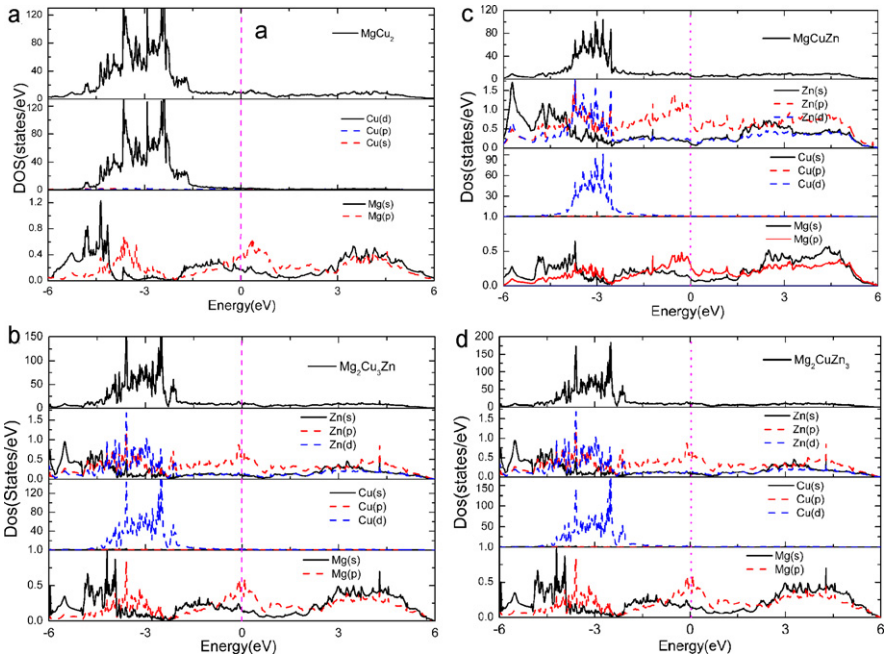

Fig. 3. The total and partial density of states (DOSs) for $MgCu_2$ (a), Mg_2Cu_3Zn (b), MgCuZn (c) and Mg_2CuZn_3 (d).

Both below and above the Fermi level, the hybridization between Cu-d states, Zn-p states and Mg-p states was strong. It should be noted that there was a pseudogap close to the Fermi level (E_F) in the total DOS of these $Mg(Cu_{1-x}Zn_x)_2$ alloys, which indicated the presence of covalent bonding. Quite often the pseudogap separated the bonding states from the anti-bonding/nonbonding states. The DOSs in Fig. 3 showed that the Fermi level fell below the pseudogap of $Mg(Cu_{1-x}Zn_x)_2$ alloys, which indicated that not all the bonding states were filled and some extra electrons were required to reach maximum stability in these alloys [42,43].

To gain more insight into the bonding behavior of these alloys we have given the contour plots of charge density on the (1 0 0) plane in Fig. 4. The contour lines were plotted from 0.02 to 0.32 e/Å^3 with 0.015 e/Å^3 interval. Higher density region corresponding to the core electron distribution of Mg, Zn and Cu atoms was omitted due to little contribution to the bonding. Fig. 4 shows that Mg atoms were almost spherical, while Cu and Zn atoms were slightly deformed. The obvious overlaps of electron densities between Cu–Cu, Zn–Zn, Zn–Cu indicated the covalent bonds between them, and these covalent bonds became weak with Zn content

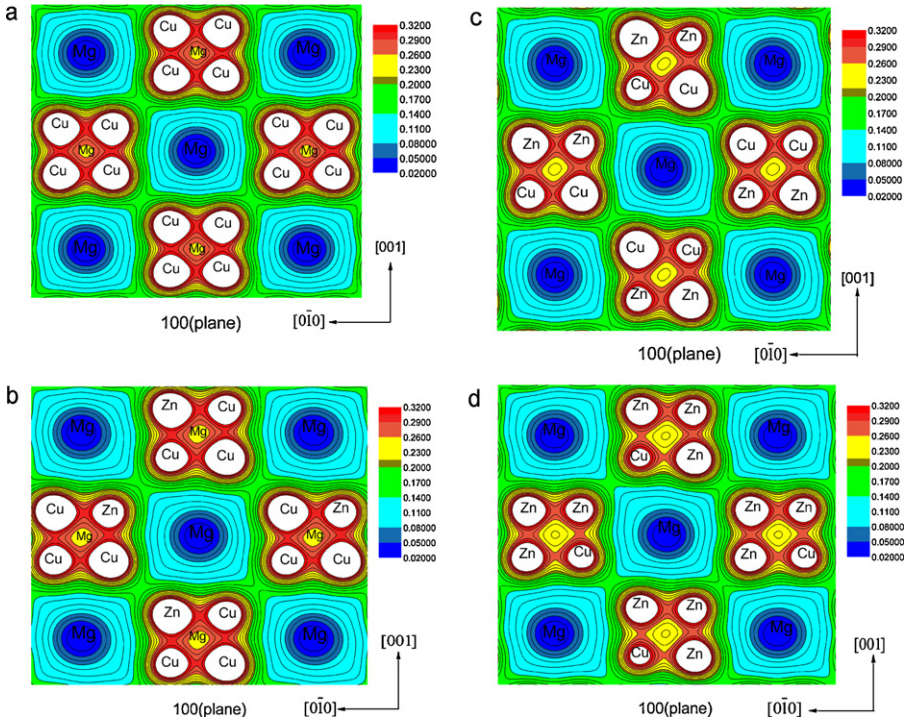

Fig. 4. The contour plots charge density on the (1 0 0) plane for $MgCu_2$ (a), Mg_2Cu_3Zn (b), MgCuZn (c) and Mg_2CuZn_3 (d).

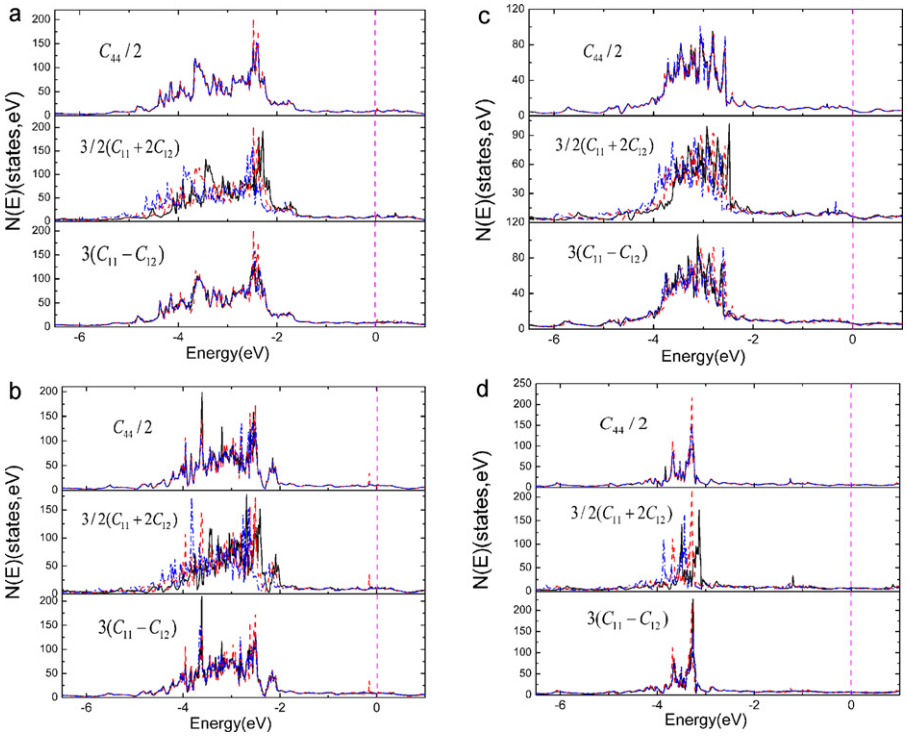

Fig. 5. The density of states for various strains of $MgCu_2$ (a), Mg_2Cu_3Zn (b), MgCuZn (c) and Mg_2CuZn_3 (d). The red line corresponds to an undistorted lattice, blue line corresponds to a −2% distortion, and black line corresponds to a 2% distortion. The Fermi level E_F was at zero energy. (For interpretation of the references to color in this figure legend, the reader is referred to the web version of the article.)

increasing, suggesting the worse stability of crystal structure. Therefore, the charge density distribution could explain the structural stability of $Mg(Cu_{1-x}Zn_x)_2$ alloys reasonably. In contrast to the Cu–Cu, Zn–Zn, Zn–Cu bonding, there was no overlap of electron distribution around Mg atoms. The almost uniform electron distribution around Mg atoms was likely to be the metallic bond and can be well described by the nearly free electron model. These results were consistent with the DOS analysis described above. The calculated results of bond length showed that the atomic distance between the nearest Cu–Cu atoms was 2.49 a.u., which was smaller than the 2.59 a.u. of the nearest Zn–Zn atoms and 2.54 a.u. of the nearest Zn–Cu atoms, respectively. This result was consistent with the volume variations from Table 1.

To further reveal the underlying mechanism for elastic properties, the subtle features of DOSs during deformation were also discussed. Fig. 5 displayed the DOS at $\delta = -0.02$, 0.00 and 0.02 for three types of strains in Table 2. Here the total DOS during deformation was focused on the range from about −6.5 eV to 1.0 eV, and the rest parts were omitted due to the similar feature. The results showed that the shears corresponding to $3/2(C_{11}+C_{12})$ were not volume conserving whereas the shears corresponding to $3(C_{11}-C_{12})$ and $C_{44}/2$ were almost volume conserving. The Force Theorem [44] on calculations of elastic constants indicated that for volume conserving, the effect of electrostatic interaction energy could be neglected. For the shear corresponding to not volume conserving, the electrostatic interaction energy must be included due to nonsphericity of the charge distribution and its variation with shear [45]. The present results revealed that the elastic constant corresponding to not volume conserving was higher due to the influence of electrostatic interaction energy.

4. Conclusions

The structural, elastic and electronic properties of $Mg(Cu_{1-x}Zn_x)_2$ with fcc structures were systematically investigated by means of first-principle calculations within the framework of density functional theory (DFT). For $Mg(Cu_{1-x}Zn_x)_2$ alloys, the optimized lattice parameter a and the volume V_0 increased with Zn content, while the structural stability decreased from the energetic point of view. The single-crystal elastic constants as well as polycrystalline elastic parameters B, G, Y, ν and A had been calculated, and the results indicated that MgCuZn exhibited the largest stiffness but obvious brittleness and weak tenacity, while Mg_2Cu_3Zn showed the best ductility. The calculated electronic structures showed that the covalent bond became weak with Zn content, revealing the underlying mechanism for the structural stability of $Mg(Cu_{1-x}Zn_x)_2$ alloys. Furthermore, the elastic constant corresponding to not volume conserving was higher due to the influence of electrostatic interaction energy. The recent investigations could provide helpful guidance for future measurement and design of new magnesium alloys.

Acknowledgments

This work is supported by NSFC (50861002 and 51071053), Natural Science Foundation of Guangxi Province (0991051), Open Project of Key Laboratory of Materials Design and Preparation Technology of Hunan Province (KF0803) and the Scientific Research Foundation of Guangxi University (X071117).

References

[1] C. Potzies, K.U. Kainer, Adv. Eng. Mater. 6 (2004) 281.
[2] Z.B. Sajuri, T. Umehara, Y. Miyashita, Y. Mutoh, Adv. Eng. Mater. 5 (2003) 910.
[3] G.L. Makar, J. Kruger, Int. Mater. Rev. 38 (1993) 138.
[4] S. Schumann, H. Friedrich, Mater. Sci. Forum 51 (2003) 419.
[5] T.M. Pollock, Science 328 (2010) 986.
[6] P. Chen, D.L. Li, J.X. Yi, B.Y. Tang, L.M. Peng, W.J. Ding, J. Alloys Compd. 485 (2009) 672.
[7] K.Q. Qiu, N.N. Hu, H.B. Zhang, W.H. Jiang, Y.L. Ren, P.K. Liaw, J. Alloys Compd. 478 (2009) 419.

[8] C. Antion, P. Donnadieu, F. Perrard, A. Deschamps, C. Tassin, A. Pisch, Acta Mater. 51 (2003) 5335.
[9] G. Nayyeri, R. Mahmudi, F. Salehi, Mater. Sci. Eng. A 527 (2010) 5353.
[10] Q. Xiang, R.Z. Wu, M.L. Zhang, J. Alloys Compd. 477 (2009) 832.
[11] M. Azimi, G.H. Akbari, J. Alloys Compd. 509 (2011) 27.
[12] M.-M. Wu, L. Wen, B.-Y. Tang, L.-M. Peng, W.-J. Ding, J. Alloys Compd. 506 (2010) 412.
[13] T. Honma, T. Ohkubo, K. Hono, S. Kamado, Mater. Sci. Eng. A 395 (2005) 301.
[14] G.A. Song, J.S. Lee, J.S. Park, N.S. Lee, W.H. Lee, J. Alloys Compd. 481 (2009) 135.
[15] M.R. Barati, J. Alloys Compd. 478 (2009) 375.
[16] R. Chaim, J. Pelleg, M. Talianker, J. Mater. Sci. 22 (1987) 1609.
[17] P. Ravindran, L. Fast, P.A. Korzhavyi, B. Johansson, J. Appl. Phys. 84 (1998) 4891.
[18] N.A. Noor, N. Ikram, S. Ali, S. Nazir, S.M. Alay-e-Abbas, A. Shaukat, J. Alloys Compd. 507 (2010) 356.
[19] C. Jiang, D.J. Sordelet, B. Gleeson, Acta Mater. 54 (2006) 2361.
[20] B.Y. Tang, N. Wang, W.Y. Yu, X.Q. Zeng, W.J. Ding, Acta Mater. 56 (2008) 3353.
[21] W.A. Counts, M. Friák, D. Raabe, J. Neuqebauer, Acta Mater. 57 (2009) 69.
[22] A. Datta, U.V. Waqhmare, U. Ramamurty, Acta Mater. 56 (2008) 2531.
[23] M.-M. Wu, B.-Y. Tang, L.-M. Peng, W.-J. Ding, Physics B 405 (2010) 4812.
[24] P. Hohenberg, W. Kohn, Phys. Rev. B 136 (1964) B864.
[25] G. Kresse, J. Furthmüller, Phys. Rev. B 54 (1996) 11169.
[26] G. Kresse, D. Joubert, Phys. Rev. B 59 (1999) 1758.
[27] P.E. Blöchl, Phys. Rev. B 50 (1994) 17953.
[28] H.J. Monkhorst, J.D. Pack, Phys. Rev. B 13 (1976) 5188.
[29] P.E. Blöchl, O. Jepsen, O.K. Andersen, Phys. Rev. B 49 (1994) 16223.
[30] S. Ganeshan, S.L. Shang, H. Zhang, Y. Wang, M. Mantina, Z.K. Liu, Intermetallics 17 (2009) 313.
[31] G.W. Shannette, J.F. Smith, J. Appl. Phys. 42 (1971) 2799.
[32] F. Birch, J. Geophys. Res. 83 (1978) 1257.
[33] Y. Kubota, M. Takata, M. Sakata, T. Ohba, K. Kifune, T. Tadaki, J. Phys.: Condens. Matter 12 (2000) 1253.
[34] M. Mattesini, R. Ahuja, B. Johansson, Phys. Rev. B 68 (2003) 184108.
[35] H.M. Ledbetter, J. Appl. Phys. 44 (1973) 1451.
[36] A. Taga, L. Vitos, B. Johansson, G. Grimvall, Phys. Rev. B 71 (2005) 014201.
[37] S.F. Pugh, Phil. Mag. Ser. 7 45 (1954) 823.
[38] D. Raabe, B. Sander, M. Friák, D. Ma, J. Neugebauer, Acta Mater. 55 (2007) 4475.
[39] W.A. Counts, M. Friák, C.C. Battaile, D. Raabe, J. Neugebauer, Phys. Status Solidi B 245 (2008) 2644.
[40] V. Tvergaard, J.W. Hutchinson, J. Am. Ceram. Soc. 71 (1988) 157.
[41] B.B. Karki, L. Stixrude, S.J. Clark, M.C. Warren, G.J. Ackland, J. Crain, Am. Mineral. 82 (1997) 51.
[42] J.H. Xu, T. Oguchi, A.J. Freeman, Phys. Rev. B 35 (1987) 6940.
[43] P. Ravindran, G. Subramoniam, R. Asokamani, Phys. Rev. B 53 (1996) 1129.
[44] A.R. Mackintosh, O.K. Andersen, Solid State Phys. 35 (1980) 1.
[45] N.E. Christensen, Solid State Commun. 49 (1984) 701.